Synthesis, characterisation and slurry phase ethylene polymerisation of *rac*-(^{Ph}BBI*)$ZrCl_2$ immobilised on modified layered double hydroxides

Grace E. Hickman, Christopher M. R. Wright, Alexander F. R. Kilpatrick, Zoë R. Turner, Jean-Charles Buffet and Dermot O'Hare*

Chemistry Research Laboratory, Department of Chemistry, University of Oxford,
12 Mansfield Road, OX1 3TA, UK

Corresponding author: dermot.ohare@chem.ox.ac.uk

Keywords: metallocene, boron-bridged, polymerisation, ethylene, layered double hydroxide

ABSTRACT

Rac- and *meso*-bis(1-hexamethylindenyl)phenylborane zirconium dichloride, {*rac*-, *meso*-(^{Ph}BBI*)$ZrCl_2$} has been synthesised and fully characterised. The slurry phase ethylene polymerisation performance of *rac*-(^{Ph}BBI*)$ZrCl_2$ immobilised on a range of methylaluminoxane (MAO)-modified, solvent-dispersed, high surface area layered double hydroxides (AMO/AIM-Mg_xAl-CO_3 LDHs) have been studied. The polymerisation activities show a strong dependence on the nature of the LDH. *Rac*-(^{Ph}BBI*)$ZrCl_2$ supported on a MAO-modified 1-hexanol dispersed $[Mg_{0.73}Al_{0.27}(OH)_2][CO_3]_{0.135}$ LDH displayed a maximum ethylene polymerisation activity of 6641 $kg_{PE}\ mol_{Zr}^{-1}\ h^{-1}\ bar^{-1}$ at 70 °C and 2 bar ethylene. Benchmarking studies reveal that some of the *rac*-(^{Ph}BBI*)$ZrCl_2$ supported catalysts outperform a range of commonly used industrial metallocene PE catalysts.

1. Introduction

Polyolefins play a vital role in today's world, with polyethylene production estimated to reach 99.6 million metric tons in 2018.[1] Titanium based Ziegler-Natta,[2] and chromium based Phillips[3] catalytic systems dominate the field of ethylene and α-olefin polymerisation. Heterogeneous catalysts limit reactor fouling with respect to homogeneous catalysts, and so are typically the commercial option. However, they have poorly understood active species, often leading to a distribution of products. Homogeneous catalysts have well defined active sites compared to heterogeneous catalysts and can offer higher selectivities.[4,5] Group 4 bent

metallocenes, Cp_2MX_2 (Cp = η-C_5H_5, M = Ti, Zr or Hf, X = Cl or alkyl group), provide an alternative to Ziegler-Natta and Phillips catalysts for ethylene polymerisation, with their single active site capable of producing polymer with narrow molecular weight distributions.[6] It has been demonstrated that variations in both the steric and electronic properties have profound effects on both the catalytic activity and the physicochemical properties of the polymers produced.[7,8]

A variety of permethylindenyl ($C_9Me_7^-$, Ind*, I*) complexes have been synthesised, including those of group 4 metals.[9-12] Ind* ligation produces a more electron rich metal centre than indenyl (Ind) due to a positive inductive effect, which strengthens the metal−ligand bonding interactions. Complexes with Ind* ligands are more sterically demanding than the parent indenyl ligand, increasing the kinetic stability of the Ind*−metal bonds.[9] These factors have been linked to improved polymerisation activity, with *rac*-ethylenebis(permethylindenyl) zirconium dichloride (*rac*-(EBI*)$ZrCl_2$) having a greater slurry phase activity (4325 $kg_{PE}\,mol_{Zr}^{-1}\,h^{-1}\,bar^{-1}$) than *rac*-ethylenebis(indenyl) zirconium dichloride (*rac*-(EBI)$ZrCl_2$; 1841 $kg_{PE}\,mol_{Zr}^{-1}\,h^{-1}\,bar^{-1}$) when both complexes were immobilised on MAO activated aqueous miscible organic layered double hydroxide (AMO-LDH) solid supports.[12]

Boron-bridged metallocene complexes have been reported by Reetz,[13a,b] Shapiro,[13c] Braunschweig,[13d] Stephan[13e] and reviewed by Bourissou *et al.*.[14] *rac*-(^{Ph,Et_2O}BBI)$ZrCl_2$, reported by Reetz *et al.*, has shown fairly active solution phase ethylene polymerisation (200−2600 $kg_{PE}\,mol_{Zr}^{-1}\,h^{-1}\,bar^{-1}$) and produced high molecular weight polymer (*ca.* 700 $kg\,mol^{-1}$).[13a]

In 1980, Kaminsky and co-workers reported that group 4 metallocenes, which have low solution phase ethylene polymerisation activity, displayed improved activity when they were activated by methylaluminoxane (MAO).[2] Although precise details about the structure and functionality of MAO remain unclear,[15] MAO is currently understood to act as a source of $[AlMe_2]^+$,[16–19] which plays a key role in transforming solution phase catalyst precursors into the catalytically active cationic species.[20] MAO has a similar importance in supported metallocene catalysis. 3rd generation Ziegler-Natta catalysts ($TiCl_4$ systems)[21,22] and Phillips catalysts[3] both involve complexes immobilised on inorganic supports, such as $MgCl_2$ and SiO_2. However, inorganic supports such as SiO_2,[23] Al_2O_3,[24] clays,[25] ZrO_2,[26] $MgCl_2$[6,27] and

AMO-LDHs[28] amongst others,[29] are only viable supports for metallocenes when they either contain Lewis acid sites, such as those found on SiO_2−Al_2O_3,[5] or are first activated, for example by coating them with MAO. The surface functional groups on the inorganic supports graft the activators such as methylaluminoxane, forming an active support,[30] which then coordinates to a metal complexes, abstracting a ligand to create the catalytically active cationic species.[31] Weckhuysen *et al.* have recently proposed that, similar to $[AlMe_2]^+$ in solution phase catalysis, silica-MAO supports have weak Lewis acidic sites which coordinate to a metallocene precursor to form the catalytically active cationic species.[32] It has also been suggested that deactivation occurs when surface silanol groups coordinate to the metal centre. As a result, careful control of the surface hydroxyl concentration is essential to optimise a solid catalyst support.

Layered double hydroxides (LDHs) are a general class of lamellar anion exchangeable materials.[33,34] They are typically represented by the general formula $[M^{z+}_{1-x}M'^{y+}_{x}(OH)_2]^{q+}[X^{n-}]_{q/n}{\cdot}m(H_2O)$ where $z = 1$ or 2, $y = 3$ or 4, $0 < x < 1$, M and M′ can be a range of metal cations including Mg^{2+}, Ca^{2+} and Al^{3+}, and X^{n-} can be a variety of anions, such as CO_3^{2-} and SO_4^{2-}. Structurally, LDHs can be compared to brucite ($Mg(OH)_2$), which consists of edge-sharing magnesium hydroxide octahedra. Substituting some divalent ions with trivalent ions results in net positively charged layers, which are balanced by intercalated anions.[35] Interlayer water provides structural stability *via* hydrogen bonding between layers.[36] Conventional water-washed LDHs are hydrophilic and their inherent high charge density and causes the primary platelets to aggregate into non-porous stone-like particles via both electrostatic and hydrogen-bonding interactions. As a result, conventional LDHs are characterised by their low specific surface areas and their poor dispersibility in non-polar solvents. These attributes impose limits on their practical applications in area such as sorbents and catalysts and inhibits their ability for efficient and extensive surface functionalisation.[37] Recently, we have found that redispersing conventional LDHs in aqueous miscible organic (AMO) solvents can create a new class of LDHs, we have termed them: AMO-LDHs. AMO-LDHS may be described by the formula $[M^{z+}_{1-x}M'^{y+}_{x}(OH)_2]^{q+}[X^{n-}]_{q/n}{\cdot}m(H_2O){\cdot}w$(AMO-solvent).[38] Molecular dynamics simulations indicate that AMO molecules strongly interact with the LDH surface to disrupt the hydrogen bonding network.[39] AMO-LDHs are highly dispersible in non-polar solvents and exhibit N_2 BET specific surface areas up to 301 $m^2\ g^{-1}$ which represents a 26200% increase in surface area compared to conventional LDHs. In addition, AMO-LDHs are less dense than conventional LDHs, with loose bulk densities of 0.10−0.18 g mL^{-1} compared to 0.29−0.95 g mL^{-1}.[40,41] Most recently, the solvents used for

AMO dispersion have been expanded to include aqueous immiscible (AIM) solvents. AIM-LDHs also exhibit similar improvements in specific surface area, density and dispersibility in non-polar solvents compared to conventional LDHs.[42]

Herein, the synthesis of phenylborane-bis(permethylindenyl) zirconium dichloride ($(^{Ph}BBI^*)ZrCl_2$) will be discussed and its activity for ethylene polymerisation when immobilised on a series of LDHs supports will be carried out. We have investigated the effect of the AMO/AIM-LDH structure on the ethylene polymerisation activity of LDH/MAO/zirconocene systems by systematic variation of the AMO or AIM solvent treatment and Mg:Al ratio in the LDH layers.

2. Results and discussion

2.1. Synthesis and characterisation of a boron bridged zirconocene complex

2.1.1. Synthesis and characterisation of ($^{Ph}BBI^*)H_2$

$Ind^{\#}Li$ was reacted with 0.5 equivalent $PhBCl_2$ in Et_2O for 12 h, after which the reaction mixture was filtered. The filtrate was dried, and the resultant grey solid washed with pentane, producing $(^{Ph}BBI^*)H_2$ in 28% crystalline yield. The ^1H NMR spectrum of $(^{Ph}BBI^*)H_2$ shows five singlets between 1.67 and 2.35 ppm in a 3:3:3:3:6 ratio for the methyl groups (Figure S1). A resonance was observed for the indenyl methine protons at 4.18 ppm, and two multiplets at 7.35 and 8.10 ppm correspond to the *meta-*/*para-* and *ortho*-protons of the phenyl rings respectively. The $^{13}C\{^1H\}$ NMR spectrum displays resonances between 125.4 and 143.4 ppm for the aromatic indenyl carbons and at 46.8 ppm for the CH carbon. This agrees well with the results reported by Rufanov *et al.* for $(^{(Me_3Si)_3}BBI)H_2$; an allylic proton was seen at 3.28 ppm, and the indenyl carbons between 123.8 and 151.5 ppm.[43] No resonances could be observed in the $^{11}B\{^1H\}$ NMR spectrum of $(^{Ph}BBI^*)H_2$. Yellow crystals suitable for a single crystal X-ray diffraction study were grown from toluene at −30 °C. The molecular structure is shown in Figure S2 and selected bond lengths and angles are given in Table S1. The indenyl rings are almost parallel (α=12.15°) in $(^{Ph}BBI^*)H_2$, most likely due to a π stacking interaction. This effect is not observed in SBI^*H_2, which adopts a tetrahedral geometry the bridging silicon atom, and adopts a conformation where the methyl groups sit between the indenyl rings, which are almost perpendicular to each other.[12] The $B-C_{Ind}$ bond lengths observed in $(^{Ph}BBI^*)H_2$ (1.609 Å average) are similar to those in $Ind_2B(NC_5H_{10})$ (1.603 Å average). However, the B−Ph bond length (1.571(31) Å) is significantly longer than the corresponding B−N bond

(1.376(2) Å).[44] Contrary to *rac*-(^{Ph,Et_2O}BBI)$ZrCl_2$ reported by Reetz *et al.*,[13a] no ether was coordinated to the boron, most likely due to the increased steric bulk of permethylindenyl when compared to the indenyl analogue.

2.1.2. Synthesis and characterisation of (^{Ph}BBI)Li_2*

^{n}BuLi was added to (^{Ph}BBI*)H_2 in Et_2O at 0 °C and allowed to warm to room temperature and stir for 2 h. After drying *in vacuo* and washing with pentane at 0 °C, (^{Ph}BBI*)Li_2 was obtained as an orange powder in 68% yield. The ^{1}H NMR spectrum showed 6 singlets between 1.27 and 3.05 ppm corresponding to the indenyl methyl groups, a multiplet at 7.14 ppm assigned to the *meta*- and *para*- phenyl protons, and a multiplet at 8.18 ppm assigned to the *ortho*- phenyl protons (Figure S3).

2.1.3. Synthesis and characterisation of (^{Ph}BBI)$ZrCl_2$*

Compound (^{Ph}BBI*)Li_2 was combined with an equimolar amount of $ZrCl_4$ in a toluene-Et_2O mixture (30:1 v/v) and stirred for 18 h (Eq. 1). The Et_2O was expected to act as a donor group to the boron atom, as was reported in *rac*-(^{Ph,Et_2O}BBI)$ZrCl_2$.[13] The reaction was filtered, and the solvent was removed *in vacuo* to afford a red powder that was washed with pentane. Recrystallisation from toluene at −30 °C afforded single crystals of *rac*-(^{Ph}BBI*)$ZrCl_2$ suitable for X-ray diffraction. When the reaction was carried out in benzene and then recrystallised in hexane at −30 °C, red crystals were obtained in a 2:1 isomeric mixture of both *rac*- and *meso*-isomers.

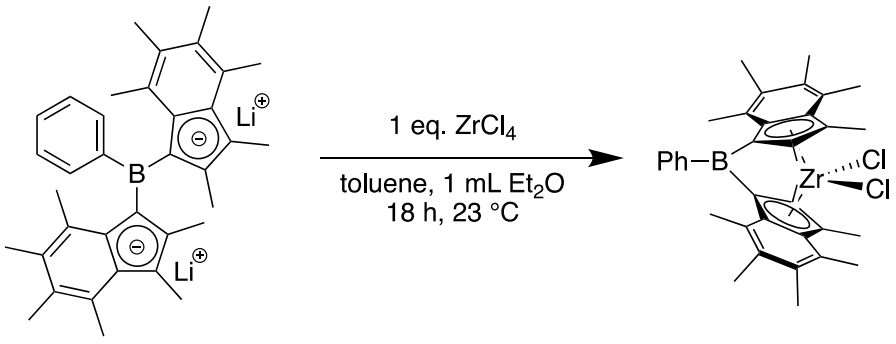

Eq. 1. Synthetic route to *rac*-(^{Ph}BBI*)$ZrCl_2$.

The ^{1}H NMR spectrum of *rac*-(^{Ph}BBI*)$ZrCl_2$ shows 6 singlets of equal intensity between 1.79 and 2.53 ppm corresponding to the six methyl groups (Figure S4). Two multiplets observed at 7.38 and 8.50 ppm were attributed to the *meta*/*para*- and *ortho*-phenyl protons respectively.

The $^{13}C\{^{1}H\}$ NMR spectrum displayed resonances between 125.8 and 133.3 ppm for the aromatic indenyl carbons. The methyl groups were observed between 15.4 and 23.4 ppm. An $^{11}B\{^{1}H\}$ signal was observed at 73.5 ppm which is at a higher frequency than in the related complexes ($^{(Me_3Si)_3C}$BBI)$ZrCl_2$ (33.2 ppm)[43] and ($^{C_5H_{10}N}$BBI)$ZrCl_2$ (38.6 ppm).[44] For ($^{C_5H_{10}N}$BBI)$ZrCl_2$, the piperidino group is doubly bonded to the boron atom; however, the large difference between the Ph- and $C(SiMe_3)_3$-substituted groups is surprising. No NMR spectroscopic data was reported by Reetz *et al.* for the analogous (^{Ph,Et_2O}BBI)$ZrCl_2$ complex. Single crystals of *rac*- and *meso*-(^{Ph}BBI*)$ZrCl_2$ were grown from toluene and hexane respectively and subject to single crystal X-ray structure analysis. The molecular structures of *rac*- and *meso*-(^{Ph}BBI*)$ZrCl_2$ are shown in Figure 1 and selected bond lengths and angles are given in Table 1.

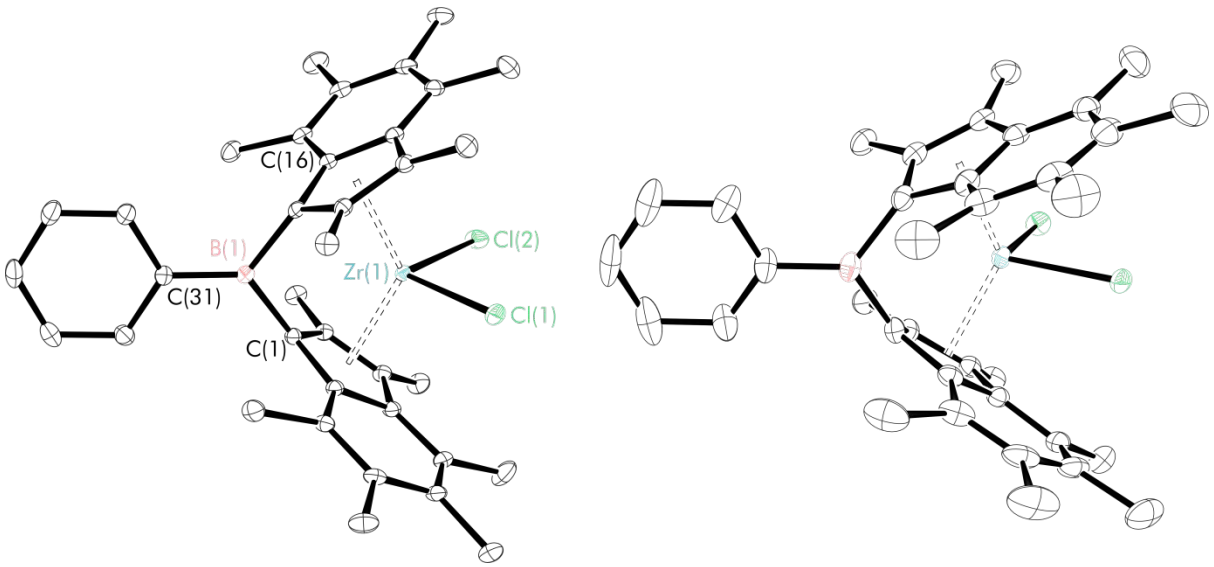

Figure 1. Solid-state molecular structures of left) *rac*- and right) *meso*-(^{Ph}BBI*)$ZrCl_2$. Thermal ellipsoids are drawn at 30% probability and hydrogen atoms have been omitted for clarity.

Table 1. Selected bond lengths and angles for *rac*- and *meso*-(^{Ph}BBI*)$ZrCl_2$. Estimated standard deviations (ESDs) are given in parentheses. ¶geometric parameters are defined in the SI.

Bond lengths and angles	*rac*-	*meso*-
Zr-B(1)/Å	3.0079	2.975
Zr-Cl(1)/Å	2.4222(4)	2.4305(12)
Zr-Cl(2)/Å	2.4209(4)	2.4053(11)
Average Zr-Cp_{Cent}/Å	2.229	2.471
C(1)-B-C(16)/(°)	107.78(13)	109.5(4)
α¶/(°)	64.67	64.54
β¶/(°)	20.06	23.56
δ¶/(°)	124.80	125.18
HA¶/(°)	3.55	4.02

The hinge and the fold angles (defined in SI) are similar to those observed in (^{Ph}BBI*)H_2. However, the Cp rings, which were almost parallel in (^{Ph}BBI*)H_2 (α=12.15°), are significantly tilted in *rac*-(^{Ph}BBI*)$ZrCl_2$ (α=64.67°) and *meso*-(^{Ph}BBI*)$ZrCl_2$ (α=64.54°). This value is larger than that reported for bis(hexamethylindenyl)zirconium dichloride, *rac*-Ind$^{\#}ZrCl_2$ (α=51.71°),[15] but similar to the value for *rac*-(^{Ph,THF}BBI)$ZrCl_2$ (α=67.61°),[13] indicating that the boron bridge results in an increase of the tilt angle of the rings. As a consequence, β is much smaller than in the proligand, but is slightly larger than that reported for *rac*-(SBI*)$ZrCl_2$ (18.69°).[12] The zirconium atom is in a distorted tetrahedral environment, as demonstrated by the distortion of the angles of Cl(1)-Zr-Cl(2) (98.689(16)°) and δ (124.80°) from the ideal value of 109.5°, most likely due to the steric bulk of the ligands in *rac*-(^{Ph}BBI*)$ZrCl_2$. The value of δ for *rac*-(^{Ph}BBI*)$ZrCl_2$ is very similar to that reported for *rac*-(^{Ph,THF}BBI)$ZrCl_2$ (122.3°),[13] but much smaller than that for *rac*-(Ind$^{\#}$)$_2ZrCl_2$, (133.59°)[45] indicating that the boron bridge reduces the steric repulsion between the indenyl rings. The average Zr-Cp_{cent} values of 2.227 Å for (*rac*-) and 2.471 Å (for *meso*-) agree well with those of other *ansa* bridged indenyl zirconocenes reported in the literature; *rac*-(SBI*)$ZrCl_2$ (2.251 Å), (EBI*)$ZrCl_2$ (2.240 Å for *rac*- and 2.246 Å for *meso*-),[12] and *rac*-(^{Ph,THF}BBI)$ZrCl_2$ (2.214 Å).[13] However, the value of $\Delta_{M\text{-}C}$ (0.212 Å average) of *rac*-(^{Ph}BBI*)$ZrCl_2$, which is similar to that for *rac*-(^{Ph,THF}BBI)$ZrCl_2$ (0.221 Å average),[13] is much larger than those of *rac*-Ind$^{\#}{}_2ZrCl_2$ (0.075 Å) and *rac*-(SBI*)$ZrCl_2$

(0.105 Å).[12] The boron bridge appears to increase the η^5–η^3 ring slip relative to other *ansa* complexes, which may impact on its reactivity profile.

2.2 Synthesis and characterisation of AMO- and AIM-Mg_zAl-CO_3 LDHs

2.2.1 Variation of the dispersing solvent

AIM- and AMO-Mg_zAl-CO_3 LDHs were prepared according to literature procedures.[40,42] They can be defined by the generalised formula, $[Mg_{1-x}Al_x(OH)_2][CO_3]_{x/2}(H_2O)_{0.23\text{-}1.0}$(AMO/AIM-solvent)$_{0.01\text{-}0.16}$ (see SI). We have adopted the abbreviation Mg_zAl-CO_3-*y*, where $z = (1–x)/x$, *y* is the AMO/AIM dispersion solvent; AMO = A (acetone), E (ethanol); AIM = T (toluene), 1H (1-hexanol) or EA (ethyl acetate).

In a typical Mg_zAl-CO_3-*y* synthesis, a 30% solid content Mg_zAl-CO_3 dispersion in water obtained by a conventional co-precipitation reaction using $Mg(NO_3)_2{\cdot}6H_2O$, $Al(NO_3)_3{\cdot}9H_2O$ and Na_2CO_3 at pH 10 is subsequently redispersed in AMO/AIM solvent (*y*) for ca. 4 hours.[42] These suspensions were then filtered and dried in a vacuum oven at room temperature for 18 h, after which they were thermally treated under vacuum at *ca*. 150 °C (Mg_3Al-CO_3-A) or 200 °C as these temperatures have been shown to maximise the polymerisation activity of catalytic systems.[28,46]

The PXRD patterns of all AMO- and AIM-Mg_3Al-CO_3-*y* LDHs (before thermal treatment; Figure 2) are similar to that of Mg_3Al-CO_3-H_2O (d_{003}=7.63 Å).[47] However, the interlayer separations (given by d_{003}) slightly increased in both the AMO- and AIM-Mg_3Al-CO_3-*y* LDHs, this slight increase in the interlayer separation appears to be independent of the dispersing solvent and may arise from less intra-layer hydrogen bonding. The lattice constants indicate that the brucite-type layer structure is retained up to 300 °C, a small decrease in the interlayer separation may indicate loss of some intercalated water or AMO/AIM solvent.[46] The peak widths at half maximum of the 003 Bragg reflections can be used to study the variation in crystallinity of the LDHs. Table S4 shows the crystalline domain lengths (CDLs) for a variety of AMO- and AIM-LDHs. If we infer that coherence along c-axis (stacking vector) is an indicator of delamination of the platelets we observe that $Mg_{2.73}Al$-CO_3-1H is the most delaminated of the LDHs, with the crystalline domain length almost a third of that of $Mg_{2.83}Al$-CO_3-T. As noted earlier, $Mg_{2.83}Al$-CO_3-T has a lower solvent content than the other LDHs, which could explain the lower extent of delamination.

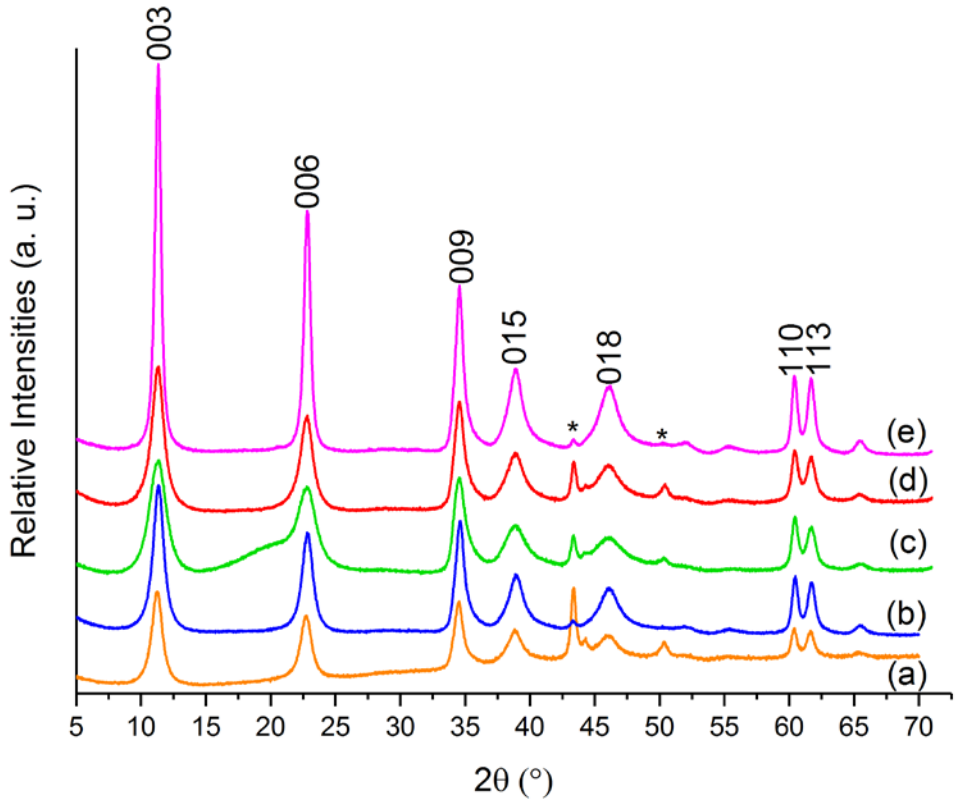

Figure 2. PXRD of AMO- and AIM-Mg_3Al-CO_3-*y* LDHs after dispersion in; (a) acetone, (b) ethanol, (c) 1-hexanol, (d) ethyl acetate and (e) toluene. (*) denotes a reflection from the sample spinner.

The AIM-LDHs display rosette morphologies (Figure 3) as expected from the co-precipitation synthesis.[40]

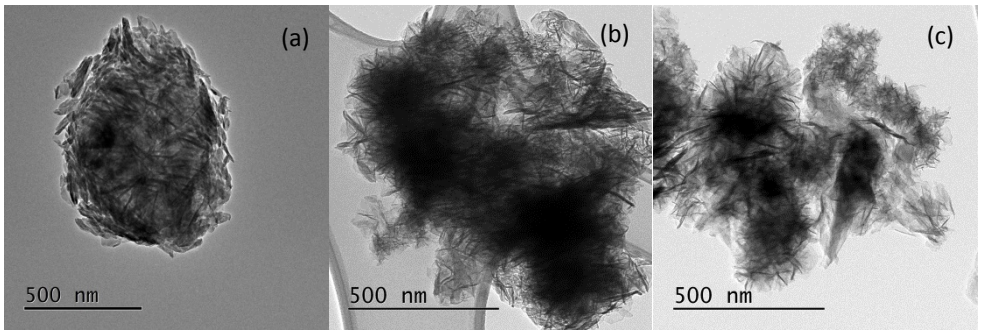

Figure 3. TEM images of (a) $Mg_{2.83}Al$-CO_3-T, (b) $Mg_{2.73}Al$-CO_3-1H and (c) $Mg_{2.94}Al$-CO_3-EA.

The disruption of the hydrogen bonding network as a result of the AMO and AIM process leads to dramatically increased specific surface areas compared to a conventional water-washed Mg_3Al-CO_3 LDH (43 $m^2\,g^{-1}$).[40]

Figure S5 shows the TGA and dTGA curves for a selection of AIM-LDHs. The toluene- and ethyl acetate-treated LDHs display two significant mass loss events, as has previously been

observed for AMO-LDHs.[46] Below the 1st minimum in the derivative (T_1; 210 and 146 °C respectively) there is a loss of coordinated surface water and AMO/AIM solvent molecules, which is followed by the formation of layered double oxides (LDOs) below the 2nd minimum in the derivative (T_2; 400 and 335 °C respectively). It can be seen that in $Mg_{2.73}Al$-CO_3-1H, these mass loss events occur, with T_1 at 150 °C and T_2 at 350 °C, however there is an additional low temperature minimum in the first derivative at 85 °C. The room temperature vacuum treatment does not appear to have successfully removed all the weakly bound 1-hexanol, resulting in the high residual solvent content, and it is proposed that it is this weakly physisorbed solvent that is lost at 85 °C.

^{27}Al, ^{1}H and ^{13}C solid state NMR (SSNMR) spectra were measured for $Mg_{2.83}Al$-CO_3-T and $Mg_{2.73}Al$-CO_3-1H before thermal treatment. The ^{27}Al spectra display only hexa-coordinated and no tetra-coordinated Al resonances,[49] with signals at 9.04 and 9.11 ppm respectively (Figures S6 and S7). ^{1}H and ^{13}C SSNMR spectra for $Mg_{2.83}Al$-CO_3-T do not show any solvent resonances (Figures S8 and S9). A maximum is seen in the ^{1}H NMR spectrum at 3.2 ppm corresponding to H_2O, and OH groups in the LDH. Only one ^{13}C resonance is observed at 169.8 ppm which is due to CO_3^{2-}. The CO_3^{2-} signal is also seen in the ^{13}C NMR spectrum for $Mg_{2.73}Al$-CO_3-1H (Figure S10) at 169.9 ppm, in addition to six signals between 13.6 and 61.9 ppm corresponding to the solvent. The ^{1}H NMR spectrum of $Mg_{2.73}Al$-CO_3-1H (Figures S11 and S12) shows four sharp resonances between 0.89 and 3.54 ppm which correspond to 1-hexanol protons. The sharpness of the signals indicates that there is still some motion off the solvent molecules, consistent with molecular dynamics simulations.[39] Superimposed on these sharp resonances, is a broad resonance can be seen which may be attributed to hydroxyl groups; Mg_3-OH groups resonate at the lower frequency, and $Mg_{1.91}Al$-OH groups have been reported to resonate around 2.4 ppm.[50] This signal is not clearly defined in the ^{1}H NMR spectrum of $Mg_{2.73}Al$-CO_3-1H, partially because it is obscured by the 1-hexanol peaks, and also because lower spinning speeds were used with respect to other literature reports.[50] An additional broad resonance is observed at 5.27 ppm, which is attributed to interlayer H_2O molecules.

2.2.2. Variation of the Mg/Al ratio in the LDH

Following the previously described procedure, $Mg_{1.91}Al$-CO_3-1H and $Mg_{3.79}Al$-CO_3-1H were synthesised from precursor solutions containing [Mg]:[Al] ratios of 2:1 and 4:1 respectively. The Mg and Al content were determined using ICP-MS. Figure 4 shows the PXRD patterns of

the Mg_xAl-CO_3-1H LDHs. There are no significant changes in the LDH structure upon changing the [Mg]:[Al] ratio.

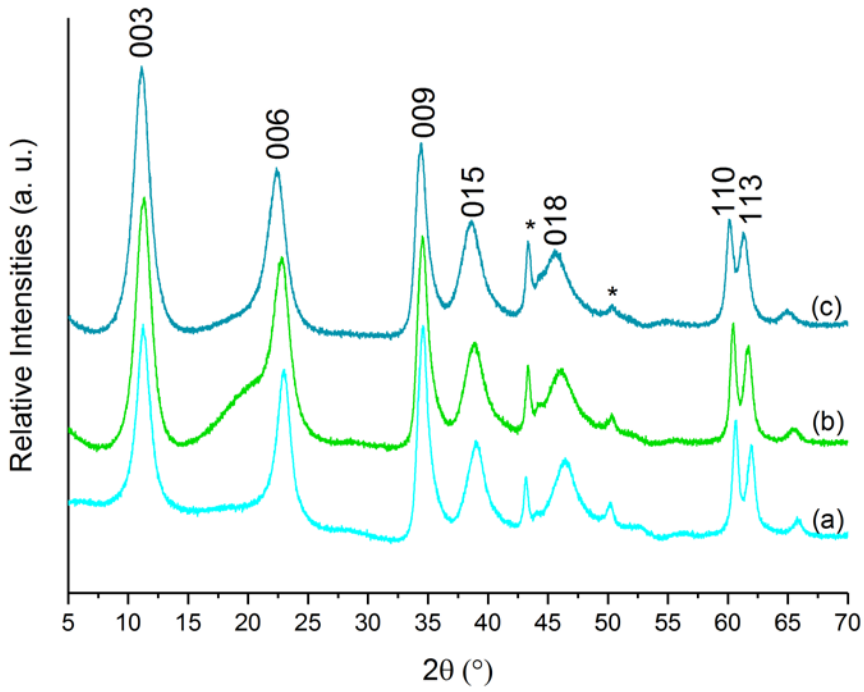

Figure 4. PXRD of (a) $Mg_{1.91}Al$-CO_3-1H, (b) $Mg_{2.73}Al$-CO_3-1H and (c) $Mg_{3.79}Al$-CO_3-1H. (*) denotes a reflection from the sample holder.

Table S6 gives the N_2 BET specific surface areas for 1-hexanol treated LDHs with varying [Mg]:[Al] ratios. $Mg_{2.73}Al$-CO_3-1H displayed the greatest specific surface area, although all the 1-hexanol-treated LDHs have greater specific surface areas than those LDHs treated with ethyl acetate or toluene. This suggests that 1-hexanol is more effective at interrupting the interlayer hydrogen bonds within LDHs and results in good delamination compared to other AIM solvents. The lower surface area observed for $Mg_{1.91}Al$-CO_3-1H may be rationalised by considering the greater electrostatic interactions associated with a higher Al content.

The TGA and dTGA curves of $Mg_{1.91}Al$-CO_3-1H and $Mg_{3.79}Al$-CO_3-1H are shown in Figure S13. Notably, these show no mass loss event in the low temperature regime (85 °C) as was observed in $Mg_{2.73}Al$-CO_3-1H, suggesting that there is less physisorption of the solvent in these LDHs. T_1 and T_2 occur at lower temperatures in $Mg_{1.91}Al$-CO_3-1H than in $Mg_{3.79}Al$-CO_3-1H; T_1 at 120 and 140 °C and T_2 at 330 and 290 °C respectively. These are both lower in turn than in $Mg_{2.73}Al$-CO_3-1H (150 and 350 °C), again implying that the solvent is bound more strongly in this LDH than in the $Mg_{1.91}Al$-CO_3-1H and $Mg_{3.79}Al$-CO_3-1H LDHs.

2.3 Slurry phase ethylene polymerisation studies

2.3.1. Synthesis and characterisation of MAO-modified Mg_xAl-CO_3 LDHs

Thermally treated AMO/AIM-Mg_xAl-CO_3 LDHs were contacted with 40 wt% MAO in toluene followed by heating at 80 °C for 2 h. The suspension was swirled frequently in order to achieve a homogeneous functionalisation by the MAO and no particle attrition. The toluene was then removed *in vacuo*. ICP-MS was used to quantify the Al wt% in $Mg_{2.73}Al$-CO_3-1H (200 °C) and $Mg_{2.73}Al$-CO_3-1H/MAO that enabled the MAO:LDH loading to be determined to be 49.4%. Diffuse reflectance Fourier transform infrared spectroscopy (DRIFTS) was used to study the acetone-, ethanol- and toluene-washed LDH materials and LDH/MAO activated supports (Figure S14). The spectra of Mg_3Al-CO_3-A and Mg_3Al-CO_3-A/MAO are shown in Figure S15 as a representative example. Absorption bands were observed assigned to CO_3^{2-} stretches (1700−1250 cm^{-1}) and OH stretches (3700−3000 cm^{-1}). Upon contacting with MAO, two IR bands, one at 2949 cm^{-1} attributed to stretching vibrations in an "Al–CH_3" moiety,[51] and one at 1219 cm^{-1} assigned to terminal methyl groups are observed.[52]

^{11}B, ^{27}Al, and ^{13}C solid state NMR (SSNMR) spectroscopy was used to study the $Mg_{2.73}Al$-CO_3-1H/MAO/*rac*-(^{Ph}BBI*)$ZrCl_2$ solid catalyst (Figure S17−S19). The ^{11}B NMR spectrum showed two B environments (17 and 22 ppm). The ^{27}Al spectrum showed octahedral Al sites, as well as the formation of a tetrahedral site.[53] The expected broad MAO resonance is possibly obscured by these sharp peaks. The ^{13}C NMR spectrum shows resonances corresponding to the phenyl protons on the ligand at 130 ppm, as well as signals between 13 and 36 ppm which may correspond to both the AIM-solvent and indenyl methyl groups. A sharp resonance at 8 ppm corresponds to MAO.

We have previously demonstrated that the surface area did not change when going from an acetone dispersed AMO-LDHs (Mg_3Al-CO_3-A) to a *rac*-(EBI)$ZrCl_2$ supported methylaluminoxane modified AMO-LDH (Mg_3Al-CO_3-A/MAO/*rac*-(EBI)$ZrCl_2$, 101 and 114 $m^2\ g^{-1}$ respectively). However, the pore volume did dramatically decrease (0.305 and 0.013 $m^3\ g^{-1}$ respectively).[28]

A Zr K-edge EXAFS study has shown that when *rac*-(EBI)$ZrCl_2$ was supported on MAO-modified AMO-LDH, the zirconium was in a tetrahedral environment with the (EBI) ligand, a methyl and in close contact with an oxygen atom from the surface.[28a]

2.3.2. Slurry phase polymerisation using immobilised zirconocenes

In an initial study, we have investigated the catalytic polymerisation activities of a series of commercial benchmark zirconocenes; $(Cp^{Me_4})_2ZrCl_2$, $(Cp^{^nBu})_2ZrCl_2$ and *rac*-(EBI)$ZrCl_2$ immobilised on a series of MAO-modified AMO- and AIM-LDHs. The zirconocenes were immobilised onto the MAO-activated AMO-/ AIM-LDH-Mg_xAl-CO_3 supports by adding a toluene solution of the zirconocenes to a toluene dispersion of the LDH and heating to 60 °C for 1 h with regular swirling. After 1 hour, the toluene supernatant solution become colourless and was removed by filtration to produce coloured solids that were dried *in vacuo* and isolated in quantitative yields..

Slurry phase ethylene polymerisation studies of $(Cp^{Me_4})_2ZrCl_2$ immobilised on five different LDHs is shown in Figure 5. The data reveal an almost tenfold increase in the polymerisation activity of $(Cp^{Me_4})_2ZrCl_2$ immobilised on $Mg_{2.73}Al$-CO_3-1H/MAO compared to $Mg_{2.94}Al$-CO_3-EA/MAO (5147 and 579 $kg_{PE}\ mol_{Zr}^{-1}\ h^{-1}\ bar^{-1}$ at 60 °C respectively). Remarkably, the nature of the LDH has significant effect on the performance of these single site metallocene catalysts. Although, they all have similar Mg:Al ratio, the dispersing solvent generates very different surface chemistry.

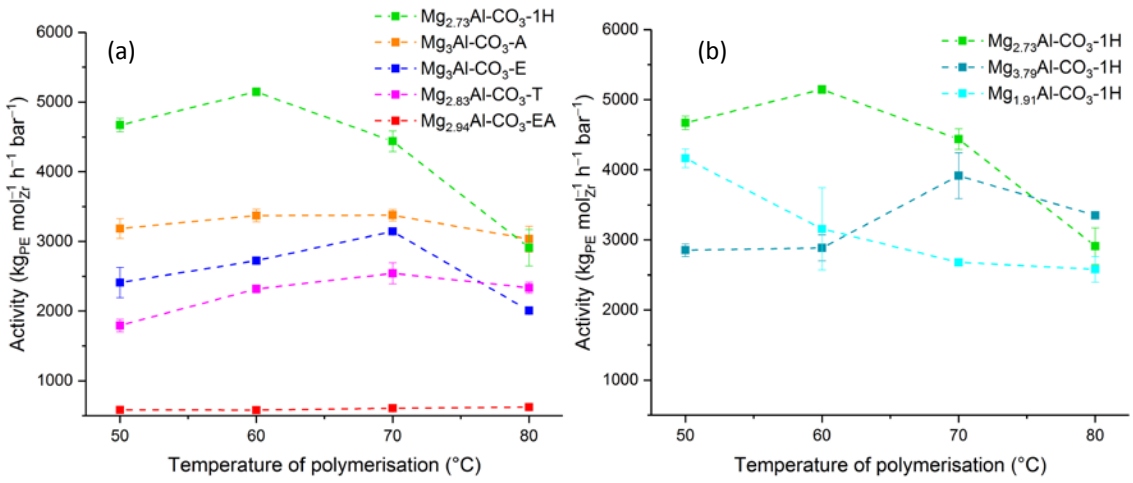

Figure 5. (a) Temperature dependence of polymerisation activity for $(Cp^{Me_4})_2ZrCl_2$ supported on a range of MAO-modified Mg_3Al-CO_3-*y* LDHs; (b) temperature dependence of polymerisation activity for $(Cp^{Me_4})_2ZrCl_2$ supported on different MAO-modified Mg_xAl-CO_3-1H LDHs. $[Al]_0$:$[Zr]_0$=100:1, TIBA cocatalyst (150 mg), 2 bar ethylene, 10 mg catalyst, 50 mL hexane and 30 minutes. Error bars given as the standard error, $\sigma_{\bar{x}} = \sigma/\sqrt{n}$.

To further examine this trend, we have studied the performance of both $(Cp^{^nBu})_2ZrCl_2$ and *rac*-(EBI)$ZrCl_2$ immobilised on $Mg_{2.73}Al$-CO_3-1H/MAO, $Mg_{2.83}Al$-CO_3-T/MAO and $Mg_{2.94}Al$-CO_3-EA/MAO. Both these complex shows the same trends (Figure S20). For example, the performance of both systems is dependent on the activated support, with again

$Mg_{2.73}Al\text{-}CO_3$-1H/MAO being the most active and $Mg_{2.94}Al\text{-}CO_3$-EA/MAO the least active support in all cases.

Rationalisation of the effect of the dispersing solvent effect is not immediately apparent, we have found no direct correlation with any physical property. It is logical that the surface area should play a role; a larger specific surface area could contribute to a more effective functionalisation by MAO and metallocene binding, improving the dispersion of the active sites and reducing the chance of a bimolecular deactivation.[5] However, we note that $Mg_{2.83}Al\text{-}CO_3$-T has a relatively low specific surface area. 1-hexanol dispersed LDHs are consistently the best supports, it may be significant that these LDHs contain high levels of residual 1-hexanol even after thermal treatment. Perhaps the presence of a small amount of 1-hexanol contributes to some additional functionalisation of the MAO with beneficial aluminium-alkoxide groups.

The performance of $(Cp^{Me_4})_2ZrCl_2$ immobilised on $Mg_{1.91}Al\text{-}CO_3$-1H LDH/MAO and $Mg_{3.79}Al\text{-}CO_3$-1H LDH/MAO were investigated to study the effect of varying the Mg:Al ratio on polymerisation activity (Figure 5b). All 1-hexanol-treated LDHs were found to be highly active supports, with $Mg_{2.73}Al\text{-}CO_3$-1H/MAO being the most active. The peak activities for the $Mg_{1.91}Al\text{-}CO_3$-1H/MAO and $Mg_{3.79}Al\text{-}CO_3$-1H supported systems were 4164 (50 °C) and 3916 $kg_{PE}\ mol_{Zr}^{-1}\ h^{-1}\ bar^{-1}$ (70 °C) respectively; lower than the $Mg_{2.73}Al\text{-}CO_3$-1H/MAO system at the same temperatures (4671 and 4438 $kg_{PE}\ mol_{Zr}^{-1}\ h^{-1}\ bar^{-1}$ at 50 and 70 °C respectively). The higher activity of $Mg_{2.73}Al\text{-}CO_3$-1H/MAO does correlate with its higher BET surface area (Table S5). Despite the higher specific surface area of $Mg_{3.79}Al\text{-}CO_3$-1H/MAO compared to $Mg_{1.91}Al\text{-}CO_3$-1H/MAO, it does not appear to be a more active catalytic support. It is possible that the higher Al^{3+} content in the latter increases the number of Lewis acidic sites, which has previously been reported to increases catalytic activity.[54] These 1-hexanol-treated LDHs produce significantly more active solid catalysts than the ubiquitous silica supports. For example, immobilisation of $(Cp^{n_{Bu}})_2ZrCl_2$ on silica that has been thermally treated at 600 °C and then modified with MAO to give SiO_2/MAO/$(Cp^{n_{Bu}})_2ZrCl_2$ produces a solid ethylene polymerisation catalyst with a peak activity of 51 $kg_{PE}\ mol_{Zr}^{-1}\ h^{-1}\ bar^{-1}$ (80 °C; 8 bar ethylene).[55]

The polymerisation activity of *rac*-(^{Ph}BBI*)$ZrCl_2$ immobilised on the MAO-functionalised AMO-/AIM-LDHs was studied and compared to the previously studied benchmark

metallocenes. A toluene solution of *rac*-(^{Ph}BBI*)$ZrCl_2$ was added to a slurry of $Mg_{2.73}Al$-CO_3-1H/MAO in toluene. The suspension turned blue upon mixing and subsequently became deep purple over the course of one hour, after filtration and drying, a pale lilac powder was isolated in quantitative yield. Figure 6 shows a comparison of the ethylene polymerisation activity of *rac*-(^{Ph}BBI*)$ZrCl_2$ on $Mg_{2.73}Al$-CO_3-1H/MAO. It can be seen that at 50 °C on the $Mg_{2.73}Al$-CO_3-1H/MAO activated support, *rac*-(^{Ph}BBI*)$ZrCl_2$ has a similar activity to (Cp^{Me_4})$_2ZrCl_2$ and ($Cp^{^nBu}$)$_2ZrCl_2$; 4866, 4670 and 4862 $kg_{PE}\ mol_{Zr}^{-1}\ h^{-1}\ bar^{-1}$ respectively. At 60 °C, it is slightly less active than (Cp^{Me_4})$_2ZrCl_2$ but more active than the other benchmark complexes, but at 70 and 80 °C, *rac*-(^{Ph}BBI*)$ZrCl_2$ outperforms all the complexes tested, with a peak activity of 6641 $kg_{PE}\ mol_{Zr}^{-1}\ h^{-1}\ bar^{-1}$ compared to 4438 $kg_{PE}\ mol_{Zr}^{-1}\ h^{-1}\ bar^{-1}$ for (Cp^{Me_4})$_2ZrCl_2$, the next most active complex.

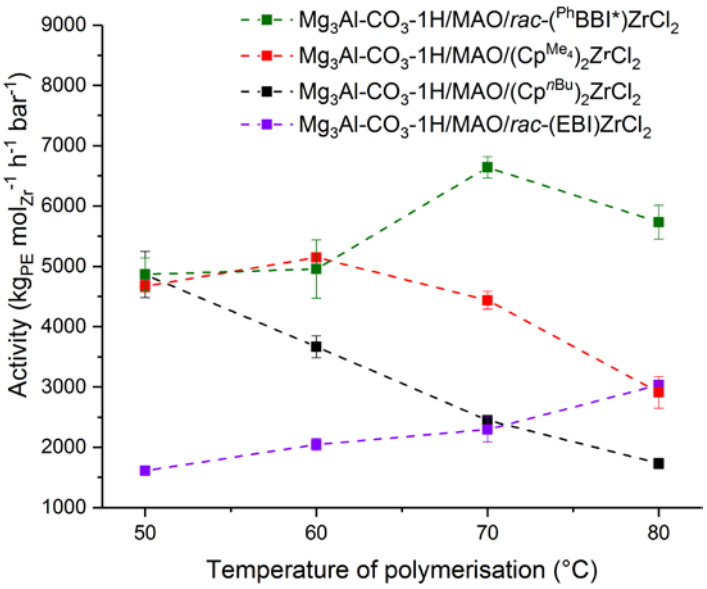

Figure 6. Temperature dependence of polymerisation activity of *rac*-(^{Ph}BBI*)$ZrCl_2$ supported on $Mg_{2.73}Al$-CO_3-1H/MAO compared to (Cp^{Me_4})$_2ZrCl_2$, ($Cp^{^nBu}$)$_2ZrCl_2$ and *rac*-(EBI)$ZrCl_2$. $[Al]_0$:$[Zr]_0$=100:1; TIBA cocatalyst (150 mg), 2 bar ethylene, 10 mg catalyst, 50 mL hexane and 30 minutes. Error bars given as the standard error, $\sigma_{\bar{x}} = \sigma/\sqrt{n}$.

The only other comparative catalytic data we could find for related B-bridged zironocenes was for *rac*-(^{Ph,Et_2O}BBI)$ZrCl_2$, in which Reetz *et al.* reported solution phase ethylene polymerisation activities between 200 and 2600 $kg_{PE}\ mol_{Zr}^{-1}h^{-1}$.[13a]

GPC analysis was used to determine the weight average molecular weights, M_w, and the number average molecular weights, M_n, of the polyethylenes (PE) produced. The M_w of the PE produced by the LDH/MAO/(Cp^{Me_4})$_2ZrCl_2$ catalyst systems are shown in Figure 7a (with the

exception of $Mg_{2.94}Al\text{-}CO_3\text{-}EA/MAO/(Cp^{Me4})_2ZrCl_2$ which did not produce enough PE for GPC analysis). The M_w of the PE produced by the AMO- and AIM-LDH/MAO systems range between 200 and 775 kg mol^{-1} and are not strongly affected by the dispersing solvent. As the polymerisation temperature increases the PE M_w decreases, which is attributed to increase rate of chain termination relative to the rate of propagation.[56]

The polydispersity index (PDI), M_w/M_n, for a single-site coordination-insertion catalyst is calculated to be 2.[30] The PDIs of the PE produced by the LDH/MAO/$(Cp^{Me4})_2ZrCl_2$ systems range from 2.65 to 3.15, which suggests a well-behaved single site behaviour (Figure 7a).

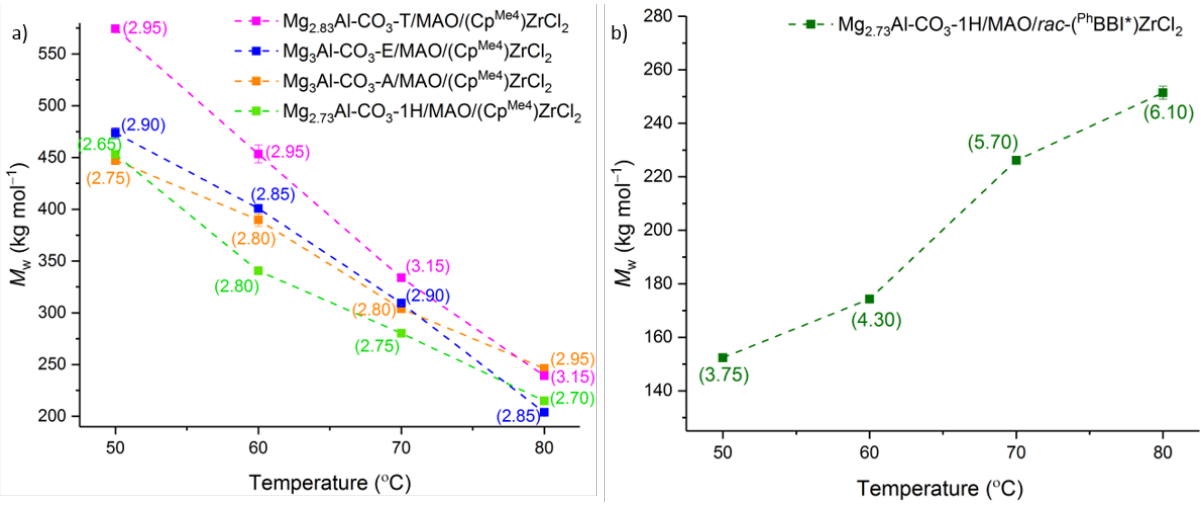

Figure 7. (a) Temperature dependence of the molecular weights of PE produced by $(Cp^{Me4})_2ZrCl_2$ supported on a range of MAO-modified $Mg_3Al\text{-}CO_3\text{-}y$ LDHs; (b) temperature dependence of the molecular weights of PE produced by *rac*-(^{Ph}BBI*)$ZrCl_2$ supported on a MAO-modified $Mg_{2.73}Al\text{-}CO_3$-1H. PDIs are given in parentheses. $[Al]_0$:$[Zr]_0$=100:1, TIBA cocatalyst (150 mg), 2 bar ethylene, 10 mg catalyst, 50 mL hexane, 30 minutes. Error bars given as the standard error, $\sigma_{\bar{x}} = \sigma/\sqrt{n}$.

The M_w of the PE produced by *rac*-(^{Ph}BBI*$ZrCl_2$) supported catalysts are shown in Figure 7b. These systems produce PE with M_w of between 150 and 250 kg mol^{-1} which are lower that those compared to the $(Cp^{Me4})_2ZrCl_2$ systems. Unusually, the M_w increases with temperature (Figure 7b), and a shoulder appears in the GPC data at higher M_w (Figure S21) as the temperature increases. This may suggest a bimodal polymerisation response, with an additional robust active site forming at high temperatures that produces higher molecular weight polymer.[57] The two ^{11}B environments observed in the SSNMR spectrum of the AIM-LDH/MAO supported complex also indicate a bimodal catalyst system. As a result the PDI values for the supported *rac*-(^{Ph}BBI*$ZrCl_2$) systems are significantly larger than the

supported $(Cp^{Me_4})_2ZrCl_2$ systems and increase with temperature, ranging from 3.75 to 6.10 when supported on LDH/MAO.

SEM images were recorded for a selection of PE samples (Figure 8). The PE produced by supported *rac*-(^{Ph}BBI*$ZrCl_2$) have more uniform popcorn morphology[58] than is often seen with PE produced using LDH/MAO activated supports.[28b]

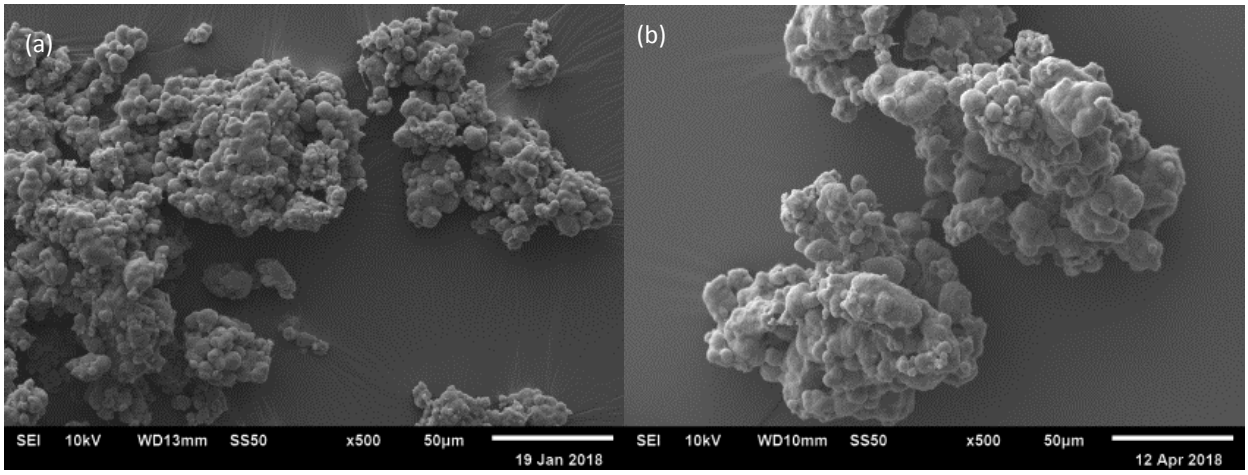

Figure 8. SEM images of polymer produced by (a) $Mg_{2.73}Al$-CO_3-1H/MAO/$(Cp^{Me_4})_2ZrCl_2$ and (b) $Mg_{2.73}Al$-CO_3-1H/MAO/*rac*-(^{Ph}BBI*)$ZrCl_2$.

3. Materials and Methods

3.1. Synthesis and characterisation of (^{Ph}BBI*)$ZrCl_2$

3.1.1. Synthesis of (^{Ph}BBI)H_2*

The synthesis of (^{Ph}BBI*)H_2 was adapted from a literature procedure.[13a] To a solution of lithium hexamethylindenyl, Ind$^{\#}$Li, (2 g, 9.70 mmol) in Et_2O (40 mL) at 0 °C, was added dropwise a solution of $PhBCl_2$ (0.6 mL, 4.79 mmol) in Et_2O (20 mL) at 0 °C. The suspension turned yellow and was allowed to warm to room temperature and stir for 18 h. The reaction was filtered and the residual solids were washed with Et_2O (3 x 20 mL). The combined filtrates were dried *in vacuo* and the crude solids washed with pentane at 0 °C (3 x 20 mL). The bulk yellow solid was redissolved in toluene and stored at −35 °C to afford yellow crystals suitable for X-ray diffraction analysis. A second crop of (^{Ph}BBI*)H_2 was obtained by storing the pentane washings at −35 °C. Compound (^{Ph}BBI*)H_2 was isolated in a total yield of 28% (640 mg, 1.32 mmol).

^{1}H NMR (400 MHz, C_6D_6, 298 K): δ 8.10 (2H, m, *o*-PhH), 7.35 (3H, m, *m*, *p*-PhH), 4.18 (2H, s, IndH), 2.35 (6H, s, IndMe), 2.19 (6H, s, IndMe), 2.05 (6H, s, IndMe), 1.98 (6H, s, IndMe) and 1.67 (12H, s, IndMe). ^{13}C{^{1}H} NMR (125 MHz, C_6D_6, 298 K): δ 143.4 (Ind), 137.0 (Ind), 136.5 (Ind), 133.5 (*o*-Ph), 132.3 (Ind), 131.7 (*p*-Ph), 129.1 (Ind), 128.7 (*m*-Ph), 127.6 (Ind), 125.4 (Ind), 46.8 (IndH), 18.3 (IndMe), 16.5 (IndMe), 16.2 (IndMe), 16.2 (IndMe), 15.6 (IndMe) and 15.4 (IndMe). An additional Ind ^{13}C resonance was expected, but was not observed, presumably obscured by the solvent resonance. Elemental analysis (%): expected: C 88.87, H 8.91; found: C 88.76, H 8.60.

3.1.2. Synthesis of (^{Ph}BBI)Li_2*

To a solution of (^{Ph}BBI*)H_2 (500 mg, 1.03 mmol) in Et_2O (20 mL) at 0 °C was added ^{n}BuLi (1.6 mL, 1.6 M in hexanes, 2.56 mmol) dropwise, and the reaction left to warm to room temperature and stir for 2 h. A colour change from yellow to red was observed. The solvent was removed *in vacuo* and the residues were washed with pentane at 0 °C (2 x 20 mL), to afford (^{Ph}BBI*)Li_2 as an orange powder in 68% yield (350 mg, 0.70 mmol).

^{1}H NMR (400 MHz, C_6D_5N, 298 K): δ 8.18 (2H, m, *o*-PhH), 7.14 (3H, m, *m*, *p*-PhH), 3.05 (6H, s, IndMe), 2.98 (6H, s, IndMe), 2.70 (6H, s, IndMe), 2.58 (6H, s, IndMe), 1.41 (6H, s, IndMe) and 1.27 (6H, s, IndMe). ^{7}Li NMR (156 MHz, C_6D_5N, 298 K): δ −0.74.

3.1.2. Synthesis of (^{Ph}BBI)$ZrCl_2$*

The synthesis of (^{Ph}BBI*)$ZrCl_2$ was adapted from a related literature procedure.[13a] $ZrCl_4$ (164 mg, 0.70 mmol) was added to (^{Ph}BBI*)Li_2 (350 mg, 0.70 mmol), followed by toluene (30 mL) and Et_2O (1 mL). The reaction was allowed to stir for 18 h and a colour change from pale to dark red was observed. The reaction was filtered, and the filtrate was dried under vacuum, yielding a red solid. This solid was washed with pentane (3 x 20 mL), then dissolved in a minimum volume of Et_2O and stored at −35 °C to obtain red crystals of *rac*-(^{Ph}BBI*)$ZrCl_2$, which were suitable for X-ray diffraction analysis.

When $ZrCl_4$ (164 mg, 0.70 mmol) was added to (^{Ph}BBI*)Li_2 (350 mg, 0.70 mmol), followed by benzene (30 mL) and the reaction was allowed to stir for 18 h, a colour change from pale to dark red was again observed. The reaction was dried and washed with hexane (3 x 60 mL). The reaction mixture was filtered and stored at −35 °C to obtain red crystals. ^{1}H NMR spectroscopy showed a 2:1 *rac*- to *meso*- ratio of isomers.

^{1}H NMR (*rac*-) (400 MHz, C_6D_6, 298 K): δ 8.50 (2H, m, *o*-PhH), 7.38 (3H, m, *m*-, *p*-PhH), 2.53 (6H, s, IndMe), 2.50 (6H, s, IndMe), 2.20 (6H, s, IndMe), 2.03 (6H, s, IndMe), 1.91 (6H, s, IndMe) and 1.79 (6H, s, IndMe). ^{1}H NMR (*meso*-) (400 MHz, C_6D_6, 298 K): δ 8.55 (2H, m, *o*-PhH), 7.35 (3H, m, *m*-, *p*-PhH), 2.53 (6H, s, IndMe), 2.46 (6H, s, IndMe), 2.29 (6H, s, IndMe), 2.00 (6H, s, IndMe), 1.87 (6H, s, IndMe) and 1.65 (6H, s, IndMe). ^{13}C{^{1}H} NMR (*rac*-) (125 MHz, C_6D_6, 298 K): *δ* 139.3 (*o*-Ph), 135.5 (*m*-Ph), 133.4 (Ind), 133.3 (Ind), 130.6 (Ind), 130.5 (Ind), 129.2 (Ind), 128.8 (*p*-Ph), 127.0 (Ind), 125.8 (Ind), 23.4 (IndMe), 17.3 (IndMe), 16.6 (IndMe), 16.3 (IndMe), 15.8 (IndMe) and 15.4 (IndMe). An additional two Ind ^{13}C resonances were expected, but were not observed, presumably obscured by the solvent resonance. ^{11}B{^{1}H} NMR (*rac*-) (160 MHz, C_6D_6, 298 K): δ 73.5 MS (EI) (*rac*-): predicted: *m/z* 643.1781; observed: m/z 643.1756. Elemental analysis (%) (*rac*-): expected: C 66.87, H 6.39; found: C 66.85, H 6.47.

3.2. Synthesis and characterisation of AMO-/AIM-LDHs

The synthesis of AMO- and AIM-Mg_xAl-CO_3 LDHs was adapted from literature procedures.[40,42] A metal precursor solution, A, was formed by dissolving $Mg(NO_3)_2{\cdot}6H_2O$ (10 g, 39 mmol) and $Al(NO_3)_3{\cdot}9H_2O$ (4.9 g, 13 mmol) in 50 mL H_2O. A second solution, B, was prepared by dissolving Na_2CO_3 (2.76 g, 26 mmol) in 50 mL H_2O. Solution A was added dropwise to solution B over the course of one hour. pH 10 was maintained throughout this step by dropwise addition of 4 M NaOH when necessary. After ageing 18 h, a white precipitate had formed. This was washed with H_2O until the pH had decreased to 7, at which point the wet cake solid was rinsed with the AMO or AIM solvent (250 mL), and redispersed in the same solvent (400 mL), until the solid was well dispersed. Following the dispersion step, the solid was filtered and rinsed again with the solvent (250 mL), before drying in a vacuum oven overnight at room temperature. The resultant solids were thermally treated under vacuum for 6 h at various temperatures and stored under a nitrogen atmosphere in a glovebox.

Mg_2Al-CO_3 and Mg_4Al-CO_3 LDHs were synthesised by the same method as Mg_3Al-CO_3-LDHs, using 10 g $Mg(NO_3)_2{\cdot}6H_2O$ and varying the Al content in each according to the desired product (7.32 and 3.66 g respectively). The Na_2CO_3 content was also adjusted to maintain a [Al]:[CO_3] of 2:1 (4.13 and 2.07 g respectively).

3.3. Slurry phase polymerisation of ethylene

3.3.1. Synthesis of solid catalysts

A solution of MAO in toluene was contacted with all the AMO-, AIM-Mg_xAl-CO_3-y LDHs prior to zirconocene immobilisation. 40 wt% MAO (200 mg) was added to each thermally treated LDH (500 mg). Toluene (40 mL) was added and the suspension was heated to 80 °C, and swirled every 10 minutes for 2 h, until the supernatant solution was clear and colourless. The solvent was removed under reduced pressure and the residual white solid dried in vacuo to give Mg_xAl-CO_3-*y* LDH/MAO.

In a typical procedure, the activated support (Mg_xAl-CO_3-*y* LDH/MAO, 200 mg, 0.98 $mmol_{Al}$;) and the zirconocene complex (4.8 mg, 0.00984 $mmol_{Zr}$) were first added to a flask. Toluene was then added and the reaction mixture was heated to 60 °C, and swirled every 10 minutes for 1 h until the supernatant solution was clear and colourless. The supernatant solution was removed by filtration and the solid supported catalyst dried *in vacuo*. A 100:1 [Al]:[Zr] was used for AMO- and AIM-Mg_xAl-CO_3-*y* LDH/MAO supported complexes.

3.3.2. Slurry phase polymerisation of ethylene

Slurry phase ethylene polymerisation studies were carried out using 10 mg catalyst precursor and 50 mL hexane in the presence of 150 mg TIBA in a 150 mL high-pressure Rotaflo ampoule. Polymerisation reactions were carried out under 2 bar overpressure of ethylene gas at various temperatures for 30 minutes. Polymerisations were stopped by removing the ampoules from the oil bath and degassing *in vacuo*. The PE produced were isolated and washed with pentane (50 mL). Each polymerisation study was conducted at least twice to determine a mean activity (quoted in units of $kg_{PE}\,mol_{Zr}^{-1}\,h^{-1}\,bar^{-1}$) and ensure reproducibility of the results.

3.4 X-ray crystallography

The solid state structures of (^{Ph}BBI*)H_2 and *rac*- and *meso*-(^{Ph}BBI*)$ZrCl_2$ have been deposited in the Cambridge Structural Database with CCDC numbers 1886090-1886092.

4. Conclusions

Boron-bridged bis-permethylindenyl zirconium complexes *rac*- and *meso*-(^{Ph}BBI*)$ZrCl_2$ have been successfully synthesised and fully characterised. The AMO and AIM-Mg_yAl-CO_3 LDHs; Mg_3Al-CO_3-A, Mg_3Al-CO_3-E, $Mg_{2.83}Al$-CO_3-T, $Mg_{2.73}Al$-CO_3-1H, $Mg_{2.94}Al$-CO_3-EA, $Mg_{1.91}Al$-CO_3-1H and $Mg_{3.79}Al$-CO_3-1H were modified with MAO and evaluated as solid

supports for a range of zirconocene precursors for slurry-phase ethylene polymerisation. The slurry-phase ethylene polymerisation activity of the immobilised zirconocenes showed a strong dependence on the nature of the $Mg_xAl\text{-}CO_3\text{-}y$ LDH. A tenfold increase in ethylene polymerisation activity was observed for $(Cp^{Me_4})_2ZrCl_2$ immobilised on $Mg_{2.73}Al\text{-}CO_3\text{-}1H/MAO$ compared to the equivalent immobilisation on $Mg_{2.94}Al\text{-}CO_3\text{-}EA/MAO$. GPC shows molecular weights, M_w, going down from 500 to 200 kg mol^{-1} and polydispersities, M_w/M_n, between 2 and 3.

Rac-(^{Ph}BBI*)$ZrCl_2$ was immobilised on a range of MAO modified AMO and AIM-$Mg_3Al\text{-}CO_3$ LDHs. A maximum ethylene polymerisation activity of 6641 $kg_{PE}\ mol_{Zr}^{-1}\ h^{-1}\ bar^{-1}$ was observed when immobilised on MAO modified $Mg_{2.73}Al\text{-}CO_3\text{-}1H$. This represents a significant improvement over the polymerisation activities observed for $(Cp^{Me_4})_2ZrCl_2$, $(Cp^{^nBu})_2ZrCl_2$ and *rac*-(EBI)$ZrCl_2$ as well as the reported values for other bridged permethylindenyl zirconocenes, *rac*-(SBI*)$ZrCl_2$ and *rac*-(EBI*)$ZrCl_2$. M_w are going up from 150 to 250 kg mol^{-1} and polydispersities are high ($3.50 < M_w/M_n < 6.10$) highlighting a system deviating from a desired metallocene single centre behaviour. Apparition of a shoulder in the GPC traces is indicative of bimodal behaviour at higher temperature which could lead to promising industrial development.

5. Notes and References

C.M.R.W., A.F.R.K., Z.R.T. (for a SCG Research fellowship) and J.-C.B. would like to thank SCG Chemicals. Co., Ltd. (Thailand) for funding. Dr. Nicholas Rees (University of Oxford) is thanked for the solid state NMR spectroscopy and Chemical crystallography (University of Oxford) for the use of the instruments.

The authors declare no conflict of interest.

1 Freedonia, *World Polyethylene - Demand and Sales Forecasts, Market Size, Market Leaders*, 2014.
2 H. Sinn and W. Kaminsky, *Adv. Organomet. Chem.*, 1980, **18**, 99–149.
3 K. H. Theopold, *Proc. Natl. Acad. Sci.*, 2014, **111**, 11578–11579.
4 T. J. Marks, *Acc. Chem. Res.*, 1992, **25**, 57–65.
5 C. Copéret, A. Comas-Vives, M. P. Conley, D. P. Estes, A. Fedorov, V. Mougel, H. Nagae, F. Núñez-Zarur and P. A. Zhizhko, *Chem. Rev.*, 2016, **116**, 323–421.
6 G. G. Hlatky, *Chem. Rev.*, 2000, **100**, 1347–1376.
7 V. Busico and R. Cipullo, *Prog. Polym. Sci.*, 2001, **26**, 443–533.

8 G. M. Benedikt and B. L. Goodall Eds, *Metallocene Catalyzed Polymers*, William Andrew Publishing, New York, 1998.
9 T. K. Miyamoto, M. Tsutsui and L.-B. Chen, *Chem. Lett.*, 1981, **10**, 729–730.
10 D. O'Hare, J. C. Green, T. Marder, S. Collins, G. Stringer, A. K. Kakkar, N. Kaltsoyannis, A. Kuhn and R. Lewis, *Organometallics*, 1992, **11**, 48–55.
11 D. O'Hare, V. Murphy, G. M. Diamond, P. L. Arnold and P. Mountford, *Organometallics*, 1994, **13**, 4689–4694.
12 J.-C. Buffet, T. A. Q. Arnold, Z. R. Turner, P. Angpanitcharoen and D. O'Hare, *RSC Adv.*, 2015, **5**, 87456–87464.
13 (a) M. T. Reetz, M. Willuhn, C. Psiorz and R. Goddard, *Chem. Commun.*, 1999, 1105–1106. (b) M. T. Reetz, R. Brummer, M. Kessler and J. Kuhnigk, *Chim. Int. J. Chem.*, 1995, **49**, 501–502. (c) P. J. Shapiro, F. Jiang, X. Jin, B. Twamley, J. T. Patton and A. Rheingold, *Eur. J. Inorg. Chem.*, 2004, 3370. (d) H. Braunschweig, M. Kraft, K. Radacki and S. Stellwag, *Z. Naturforsch.*, 2006, **61b**, 509-516. (e) H. Al-Shammari, Y. Sun, D. Stephan, S. Al Hubish and Z. Jiangtao, 2016, WO2016037960A1.
14 D. Bourissou, C. Freund, B. Martin-Vaca and G. Bouhadir, *C. R. Chimie*, 2006, **9**, 1120-1142.
15 H. S. Zijlstra and S. Harder, *Eur. J. Inorg. Chem.*, 2015, **2015**, 2.
16 L. Luo, S. A. Sangokoya, X. Wu, S. P. Diefenbach, and B. Kneale, 2009, WO2009029857A1.
17 F. Ghiotto, C. Pateraki, J. Tanskanen, J. R. Severn, N. Luehmann, A. Kusmin, J. Stellbrink, M. Linnolahti and M. Bochmann, *Organometallics*, 2013, **32**, 3354–3362.
18 T. K. Trefz, M. A. Henderson, M. Y. Wang, S. Collins and J. S. McIndoe, *Organometallics*, 2013, **32**, 3149–3152.
19 H. S. Zijlstra, M. Linnolahti, S. Collins and J. S. McIndoe, *Organometallics*, 2017, **36**, 1803–1809.
20 E. Y.-X. Chen and T. J. Marks, *Chem. Rev.*, 2000, **100**, 1391–1434.
21 P. C. Barbé, G. Cecchin and L. Noristi, in *Catalytical and Radical Polymerization*, Springer Berlin Heidelberg, Berlin, Heidelberg, 1986.
22 B. Kornelia and N. Maria, *J. Appl. Polym. Sci.*, 1998, **69**, 1005–1011.
23 P. Wongwaiwattanakul and B. Jongsomjit, *Catal. Commun.*, 2008, **10**, 118–122.
24 K. Soga and M. Kaminaka, *Die Makromol. Chemie*, 1993, **194**, 1745–1755.
25 P. A. Zapata, C. Belver, R. Quijada, P. Aranda and E. Ruiz-Hitzky, *Appl. Catal. A Gen.*, 2013, **453**, 142–150.
26 T. Pothirat, B. Jongsomjit and P. Praserthdam, *Catal. Commun.*, 2008, **9**, 1426–1431.
27 R. Huang, F. Malizia, G. Pennini, C. E. Koning and J. C. Chadwick, *Macromol. Rapid Commun.*, 2008, **29**, 1732–1738.
28 (a) J.-C. Buffet, N. Wanna, T. A. Q. Arnold, E. K. Gibson, P. P. Wells, Q. Wang, J. Tantirungrotechai and D. O'Hare, *Chem. Mater.*, 2015, **27**, 1495–1501. (b) J.-C. Buffet, Z. R. Turner, R. T. Cooper and D. O'Hare, *Polym. Chem.*, 2015, **6**, 2493–2503.
29 M. Klapper, D. Joe, S. Nietzel, J. W. Krumpfer and K. Müllen, *Chem. Mater.*, 2014, **26**, 802–819.
30 J. R. Severn, J. C. Chadwick, R. Duchateau and N. Friederichs, *Chem. Rev.*, 2005, **105**, 4073–4147.
31 R. F. Jordan, *Chemistry of Cationic Dicyclopentadienyl Group 4 Metal-Alkyl Complexes*, Academic Press, 1991, vol. 32.
32 M. E. Z. Velthoen, A. Muñoz-Murillo, A. Bouhmadi, M. Cecius. S. Diefenbach and B. M. Weckhuysen, *Macromolecules*, 2018, **51**, 343-355.
33 V. Rives, *Layered double hydroxides: present and future*, Nova Science Publishers, 2001.

34 X. Duan and D. G. Evans, *Layered Double Hydroxides*, Springer Verlag, 2006.
35 L. Pesic, S. Salipurovic, V. Markovic, D. Vucelic, W. Kagunya and W. Jones, *J. Mater. Chem.*, 1992, **2**, 1069–1073.
36 (a) F. Cavani, F. Trifirò and A. Vaccari, *Catal. Today*, 1991, **11**, 173–301. (b) L. Resconi, L. Cavallo, A. Fait and F. Piemontesi, *Chem. Rev.*, 2000, **100**, 1253–1346.
37 A. I. Khan and D. O'Hare, *J. Mater. Chem.*, 2002, **12**, 3191–3198.
38 (a) Q. Wang and D. O'Hare, *Chem. Rev.*, 2012, **112**, 4124–4155. (b) Q. Wang and D. O'Hare, *Chem. Commun.*, 2013, **49**, 6301–6303.
39 V. Erastova, M. T. Degiacomi, D. O'Hare and H. C. Greenwell, *RSC Adv.*, 2017, **7**, 5076–5083.
40 C. Chen, M. Yang, Q. Wang, J.-C. Buffet and D. O'Hare, *J. Mater. Chem. A*, 2014, **2**, 15102–15110.
41 N. P. Funnell, Q. Wang, L. Connor, M. G. Tucker, D. O'Hare and A. L. Goodwin, *Nanoscale*, 2014, **6**, 8032–8036.
42 K. Ruengkajorn, V. Erastova, J.-C. Buffet, H. C. Greenwell and D. O'Hare, *Chem. Commun.*, 2018, **54**, 4394–4397.
43 K. Rufanov, E. Avtomonov, N. Kazennova, V. Kotov, A. Khvorost, D. Lemenovskii and J. Lorberth, *J. Organomet. Chem.*, 1997, **536**–**537**, 361–373.
44 H. Braunschweig, M. Kraft, K. Radacki and S. Stellwag, *Zeitschrift für Naturforsch. B*, 2006, **61**, 509–516.
45 (a) T. A. Q. Arnold, J.-C. Buffet, Z. R. Turner and D. O'Hare, *J. Organomet. Chem.*, 2015, **792**, 55-56. (b) P. Angpanitcharoen, G. Hay, J.-C. Buffet. Z. R. Turner, T. A. Q. Arnold and D. O'Hare, *Polyhedron*, 2016, **116**, 216.
46 C. M. R. Wright, K. Ruengkajorn, A. F. R. Kilpatrick, J.-C. Buffet and D. O'Hare, *Inorg. Chem.*, 2017, **56**, 7842–7850.
47 M. Yang, O. McDermott, J.-C. Buffet and D. O'Hare, *RSC Adv.*, 2014, **4**, 51676–51682.
48 J. R. Severn and J. C. Chadwick, *Tailor-Made Polymers: Via Immobilization of Alpha-Olefin Polymerization Catalysts*, 2008.
49 G. Yu, Y. Zhou, R. Yang, M. Wang, L. Shen, Y. Li, N. Xue, X. Guo, W. Ding and L. Peng, *J. Phys. Chem. C*, 2015, **119**, 12325–12334.
50 P. J. Sideris, U. G. Nielsen, Z. Gan and C. P. Grey, *Science*, 2008, **321**, 113 LP-117.
51 V. N. Panchenko, N. V Semikolenova, I. G. Danilova, E. A. Paukshtis and V. A. Zakharov, *J. Mol. Catal. A Chem.*, 1999, **142**, 27–37.
52 J. L. Eilertsen, E. Rytter and M. Ystenes, *Vib. Spectrosc.*, 2000, **24**, 257–264.
53 G. Busca, *Catal. Today*, 1998, **41**, 191–206.
54 R. Van Grieken, A. Carrero, I. Suarez and B. Paredes, *Eur. Polym. J.*, 2007, **43**, 1267–1277.
55 M. A. Bashir, T. Vancompernolle, R. M. Gauvin, L. Delevoye, N. Merle, V. Monteil, M. Taoufik, T. F. L. McKenna and C. Boisson, *Catal. Sci. Technol.*, 2016, **6**, 2962–2974.
56 L. D'Agnillo, J. B. P. Soares and A. Penlidis, *Macromol. Chem. Phys.*, 1998, **199**, 955–962.
57 A. Ahlers and W. Kaminsky, *Die Makromol. Chemie, Rapid Commun.*, 1988, **9**, 457–461.
58 (a) J.-C. Buffet, Z. R. Turner and D. O'Hare, *Chem. Commun.*, 2018, **54**, 10970-10973. (b) T. J. Williams, J.-C. Buffet, Z. R. Turner and D. O'Hare, *Catal. Sci. Technol.*, 2018, **8**, 5454-5461. (c) J. V. Lamb, J.-C. Buffet, Z. R. Turner and D. O'Hare, *Polym. Chem.*, 2019, doi: 10.1039/C8PY01796D.
59 (a) F. P. Alt, L. L. Böhm, H.-F. Enderle and J. Berthold, *Macromol. Symp.*, 2001, **163**, 135-143. (b) J. R. Severn and J. C. Chadwick, *Dalton Trans.*, 2013, **42**, 8979-8987.